Osteoporos Int (2012) 23:377–389
DOI 10.1007/s00198-011-1812-x

ORIGINAL ARTICLE

Deletion of estrogen receptor beta accelerates early stage of bone healing in a mouse osteotomy model

Y.-X. He · Z. Liu · X.-H. Pan · T. Tang · B.-S. Guo · L.-Z. Zheng · X.-H. Xie · X.-L. Wang · K.-M. Lee · G. Li · Y.-P. Cao · L. Wei · Y. Chen · Z.-J. Yang · L.-K. Hung · L. Qin · G. Zhang

Received: 9 August 2011 / Accepted: 19 September 2011 / Published online: 27 October 2011

Abstract
Summary This study examined the role of estrogen receptor (ER) beta during mouse femoral fracture healing by employing ER knockout (KO) mice. The fracture healing in KO mice was enhanced in the early stage of neovascularization and the middle stage of endochondral ossification.
Introduction This study was conducted to examine the role of ER beta during fracture healing.
Methods Female ERbeta knockout (KO) mice (18 weeks old) and age-matched female wild-type (WT) mice underwent open osteotomy on the right femur. They were sacrificed at 1, 2, 4 and 6 weeks post-fracture. The sera and callus samples were subjected to the following analyses: micro-computed tomography (CT)-based angiography, micro-CT evaluation, histological examination, histomorphometry examination, real-time polymerase chain reaction (PCR) analysis, biochemical marker, and mechanical testing.
Results Micro-CT-based angiography showed that the total vessel volume at the fracture site was larger in the KO group than the WT group at 1 and 2 weeks post-fracture. Micro-CT analysis revealed that the callus volume was significantly higher in the KO group from week 2 to week 4 post-fracture when compared with the WT group consistent with the histological data. Analysis of biochemical markers

Y.-X. He · Z. Liu · X.-H. Pan · T. Tang · B.-S. Guo · L.-Z. Zheng · X.-H. Xie · X.-L. Wang · G. Li · L.-K. Hung · L. Qin (✉) · G. Zhang (✉)
Musculoskeletal Research Laboratory,
Department of Orthopedics and Traumatology,
The Chinese University of Hong Kong,
Shatin, Hong Kong, China
e-mail: lingqin@cuhk.edu.hk
e-mail: zhangge@ort.cuhk.edu.hk

X.-H. Pan
Department of Orthopedics, Shenzhen People's Hospital,
Medical College of Ji Nan University,
518020 Shenzhen, China

X.-L. Wang · L. Qin
Translational Medicine Research and Development Center,
Institute of Biomedical and Health Engineering,
Shenzhen Institute of Advanced Technology,
a branch of the Chinese Academy of Science,
518055 Shenzhen, China

K.-M. Lee
Lee Hysan Clinical Research Laboratory,
The Chinese University of Hong Kong,
Shatin, Hong Kong, China

Y.-P. Cao
Department of Orthopedics, Peking University First Hospital,
100034 Beijing, China

L. Wei
Department of Orthopaedics,
Warren Alpert Medical School of Brown University,
Providence, RI, USA

L. Wei
Department of Orthopaedics,
Shanxi Key Laboratory of Bone and Soft Tissue Injury Repair,
Shanxi Medical University,
Taiyuan 030001 Shanxi, China

Y. Chen
Department of Orthopedics, Shenzhen Second People's Hospital,
Futian 518035 Shenzhen, China

Z.-J. Yang
School of Chinese Medicine, Hong Kong Baptist University,
Hong Kong, SAR, China

indicated that circulating P1NP levels in the KO mice were significantly higher than in the WT mice from week 2 to week 4 and that temporal expression of circulating C-terminal telopeptide of type I collagen (CTX) levels was also higher in the KO mice than in the WT mice. These results were consistent with quantitative real-time PCR analysis. The ultimate load, stiffness, and energy to failure were significantly higher in the KO mice than in the WT mice at week 4.

Conclusions The fracture healing in KO mice was enhanced in the early stage of neovascularization and the middle stage of endochondral ossification, but not by the end of healing. Blockade of ERbeta can be considered as another therapeutic strategy for osteoporotic fracture and non-union fracture.

Keywords Estrogen receptor beta · Fracture · Mice · Micro-CT

Abbreviations

ER	Estrogen receptor
KO	Knockout
Micro-CT	Micro-computed tomography
WT	Wild-type

Introduction

Fracture healing is a specialized postnatal repair process that recapitulates of embryological skeletal development [1]. It involves a well-characterized cascade of events including three major stages. The first stage is an inflammation reaction that recruits of both immune cells and mesenchymal progenitors. The second stage is the formation of a mineralized callus in a woven bone pattern via two osteogenesis processes, i.e., the direct formation of bone through periosteal response (intramembranous ossification) and the formation of bone through a cartilage intermediate (endochondral ossification). During those two osteogenesis processes, angiogenesis is either a concurrent or a correlated process for neo-vascularization. The angiogenesis is presumed to occur mainly via initial vascular growth from feeding vessels in the periosteum. The third stage is bone remodeling from woven bone to lamellar bone until a structure similar to that prior to injury is achieved [2–4].

Estrogen is an important regulator of skeletal growth, development and maintenance [5], and it can enhance the fracture healing in mice [6]. There are two main estrogen receptor (ER) subtypes, denoted ERalpha and ERbeta [7, 8]. However, the role of these two receptors in mediating the effect of estrogen on bone healing is not fully understood.

ERbeta inhibits intramembranous and endochondral ossification as well as angiogenesis

Generations of knockout (KO) mice lacking ERalpha, ERbeta, or both provided an important tool for understanding the physiological role of each receptor subtype in skeletal growth and development. Previous studies demonstrated that female mice lacking ERbeta display an increased periosteal circumference and linear growth during both young and adult phases [9–13]. It suggested that ERbeta signaling participates in the inhibition of intramembranous ossification (radial bone growth) and endochondral ossification (linear bone growth). Additionally, breast cancer researchers found that ERbeta could reduce the expression of vascular endothelial growth factor (VEGF) messenger ribunucleic acid (mRNA) and the secretion of VEGF proteins in cell culture medium. Furthermore, transient transfect ion assays with 1,026 bp VEGF promoter constructs revealed a repressive effect of ERbeta at the promoter level of this gene. These data suggests that ERbeta signaling participates in the inhibition of angiogenesis [14].

Blockade of ERbeta signaling may promote fracture healing

Because ERbeta inhibits the three fracture healing important processes (intramembranous ossification, endochondral ossification, and angiogenesis) during fracture healing, we hypothesize that blockade of ERbeta signaling by a KO could promote fracture healing in mice. In the present study, we examined the differences in fracture healing patterns over time between ERbeta KO mice and the wild-type (WT) mice. Radiography was used to monitor fracture healing, Micro-computed tomography (CT) was employed for analysis of callus angiogenesis and structure; quantitative real-time polymerase chain reactions (PCRs) were employed for quantifying fracture healing-related gene expression in the fracture site at the mRNA level; enzyme-linked immunosorbent assays (ELISA) were performed to evaluate the serum bone turnover biochemical markers at the protein level; histology was used to describe callus histopathological features at the tissue level, and a three-point bending test was employed to determine the fracture site mechanical properties at the functional level.

Materials and methods

Experimental animals

Three pairs of ERbeta KO mice (B6.129P2-Esr2tm1Unc/J, female heterozygote×male homozygote) were purchased

from the Jackson Laboratory (Bar Harbor, ME, USA) for breeding female ERbeta KO mice. Female C57BL/6 J mice were used as WT control as suggested by Jackson Laboratory (http://jaxmice.jax.org/strain/004745). The 18-week-old female ERbeta KO mice (88) and age-matched female WT mice (88) were obtained from the accredited Laboratory Animal Services Center of the Chinese University of Hong Kong. All mice were housed and acclimatized at the research animal laboratory. The Animal Experimentation Ethics Committee of the Chinese University of Hong Kong had approved the care and experimental protocol of this study (Ref. No. 09/001/GRF).

Fracture model and experimental design

A model of mouse open femur osteotomy was used as previously reported [15]. Briefly, general anesthesia was induced by intraperitoneal injections of ketamine hydrochloride (100 mg/kg body weight) and xylazine (4 mg/kg body weight). A 10-mm longitudinal incision was made sterilely over the lateral thigh. The intramuscular septum between the vastus lateralis and the hamstring muscles was divided by blunt dissection to localize the femur. The femur was fractured at its midshaft by means of a transverse osteotomy with a bone saw. To stabilize the fracture, a 23-gauge needle was inserted retrograde into the intramedullary canal, beginning in the knee between the femoral condyles and exiting by the greater trochanter. Absorbable sutures were used to close the intramuscular septum and skin incision.

The fractured mice were sacrificed on week 1 for analyzing angiogenesis, week 2 for evaluating soft callus formation, week 4 for assessing hard callus formation, and week 6 for examining callus remodeling. Immediately after the sacrifice, sera were collected via cardiac puncture and analyzed by ELISA for bone formation and bone resorption markers and radiopaque contrast reagents (Microfil 117; Flow Tech, Carver, MA, USA.) were perfused to allow for micro-CT based angiography. Thereafter, femoral samples from each group were collected and subjected to the following analyses: four callus for micro-CT-based angiography and histological examination; another four callus for histomorphometry examination; another four callus for quantitative real-time PCR analysis of collagen type I (Col1a1), collagen type II (Col2a1), X, osteocalcin (OC), tartrate-resistant acid phosphatase (TRAP), and VEGF; and the other eight callus for microCT and three-point mechanical testing. Another eight mice without operation from each group were sacrificed to examine the baseline serum biomarkers and mRNA expression at the femoral diaphysis.

Radiographic analysis

The fracture healing process was monitored weekly by a high-resolution digital radiography system (Faxitrion MX-20, Faxitron X-ray, Illinois, USA) for a radiographic analysis with an exposure of 32 kV for 3 s. The callus area of the fractured femur was measured at each time point. Briefly, the callus was outlined as shown in Fig. 1a, and the cross-sectional area enclosed by the line was calculated using Metamorph Image Analysis System (Universal Imaging, Downingtown, PA, USA).

Micro-CT-based angiography

Micro-CT-based angiography was performed to evaluate neovascularization using our previously established protocols [16, 17]. The vasculature of each mouse was sequentially perfused at physiological pressure using heparinized (100 units/ml) normal saline, followed by 10% neutral-buffered formalin. The vascular system was injected with Microfil 117 (Flow Tech), a radiopaque, lead chromate-based contrast reagent, and was allowed to polymerize for 24 h at 4°C. The femora were isolated from the surrounding musculature, stored at 4°C for 48 h in 10% neutral-buffered formalin, transferred to a 9% formic acid solution for 48 h to decalcify the mineralized bone, washed thoroughly using water, and stored in 10% neutral-buffered formalin until imaging. The specimens were imaged using a vivaCT 40 (Scanco Medical, Switzerland) with a voltage of 70 keV, a current of 114 μA, and an isotropic resolution of 10.5 μm. A total 400 slices (200 slices above the fracture line and 200 slices below the fracture line) were selected as the volume of interest, and the two-dimensional (2D) images were globally thresholded based on X-ray attenuation before being used to construct the contrast-filled vascular network that is segmented from the surrounding tissues. The total vessel volume, average vessel diameter, and vessel volume fraction (total vessel volume divided by total volume) were calculated using built-in software [17, 18].

Micro-CT analysis of callus

After removal of soft tissues and the intramedullary pin, the harvested femora were scanned by micro-CT system (vivaCT 40, Scanco Medical) at a voltage of 70 keV with a current of 114 μA. The scan range covered 3 mm proximal and 3 mm distal to the fracture line with a resolution of 10.5 μm. The contoured regions of interest (ROIs) were selected from 2D CT images. Three-dimensional (3D) reconstructions of mineralized tissues were performed using a low-pass Gaussian filter (Sigma=1.2, Support=2). To differentiate newly formed mineralized callus from old cortices, the low- and high-density mineralized

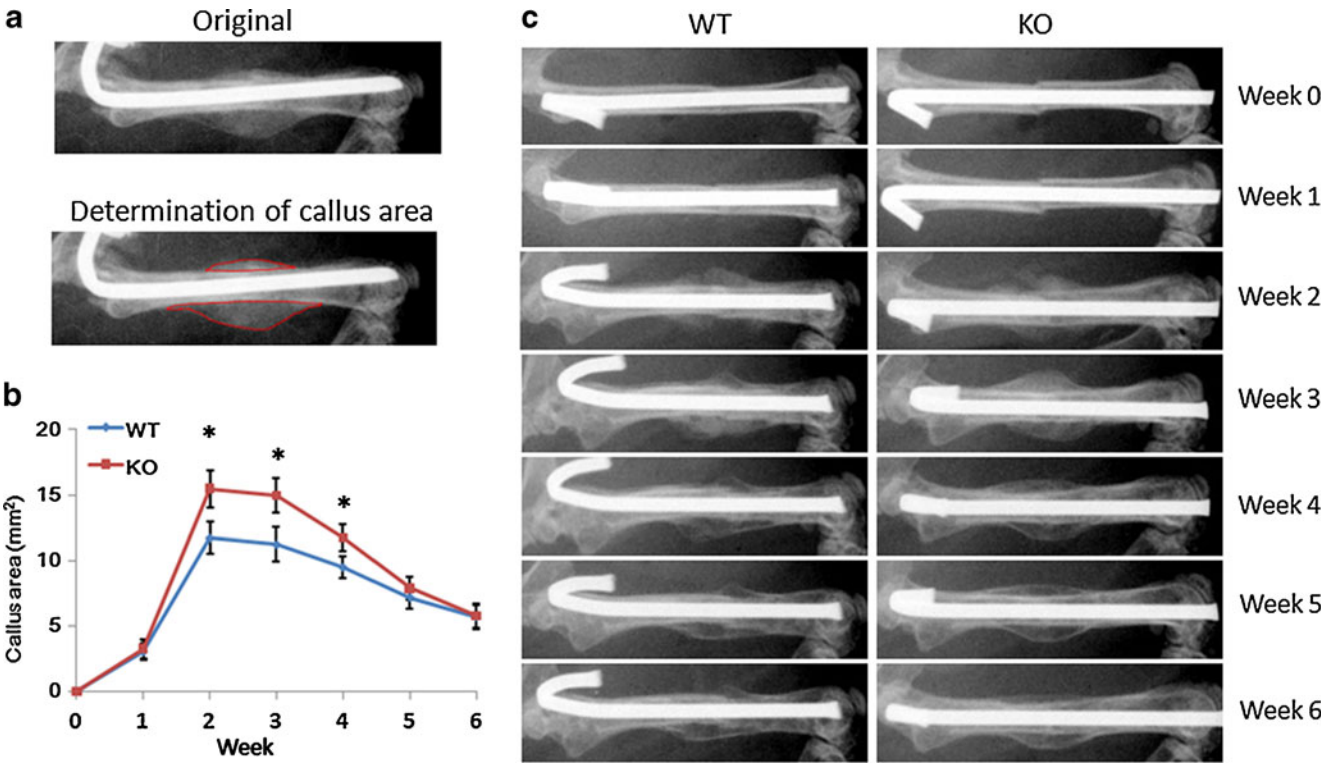

Fig. 1 Serial radiographic analysis of fracture callus. **a** Definition of ROI for callus area. **b** Quantification of callus area. **c** Longitudinal follow up of fracture healing from week 0 to week 6, with larger callus size observed in the KO mice compared with the WT mice at 2, 3, and 4 weeks post-fracture. $N=8$ for each group, $^*P<0.05$ for comparison between WT and KO group at same time point by a two-way ANOVA with a LSD post hoc test

tissues were reconstructed using different thresholds (high attenuation=250, low attenuation=130) defined in 2D images using our established evaluation protocol [19]. The high-density tissues represented old cortices and newly formed, highly mineralized callus, whereas the low-density tissues represented newly formed callus. Quantitative analysis was performed covering the middle 400 slices (200 slices above the fracture line and 200 slices below the fracture line) with the low- and high-density mineralized tissues evaluated separately. Morphometric parameters used for evaluation included total tissue volume (TV, mm^3, calculated from the contoured ROI in 2D images), volume of high-density bone (BV_h, mm^3), volume of low-density bone (BV_l, mm^3), total bone volume (BV_t, mm^3, i.e., equivalent to BV_h+BV_l, or TV-interstitial space) and normalized percentage of the tissue volumes including BV_h/TV, BV_l/TV and BV_t/TV. Apart from that, bone mineral content (BMC) was also calculated as a callus mineralization indicator.

Histological examination

Isolated femora were fixed in 10% neutral-buffered formalin, transferred to 70% ethanol, and decalcified in 9% formic acid. After tissue processing, the specimens were embedded in paraffin. Sections (5 μm) were cut sagittally along the femoral shaft axis and were collected on glass slides, deparaffinized, and subjected to hematoxylin and eosin (H&E) staining and Safranin O staining using the standard protocols. After mounting with coverslips, the specimens were viewed and analyzed under a light microscope (Leica DMRB DAS; Leica, Heerbrugg, Switzerland). For quantitative analysis, the ROI was evaluated in Safranin O-stained slides covering 1.5 mm proximal and distal to the fracture line (total 3 mm). The external callus tissues within the ROI were quantified as the total callus area (TCA), while the cartilaginous callus area (CCA) was manually defined using the Metamorph Image Analysis System (Universal Imaging; Fig. 4b). The percentage of CCA in the callus area was expressed as CCA/TCA.

Dynamic bone histomorphometric analysis

WT mice and KO mice (four for each type) were used to assess dynamic bone histomorphometry. The mice were double-labeled using a subcutaneous injection of 10 mg/kg of calcein green (Sigma Chemical, St. Louis, MO, USA) 10 days prior to sacrifice and a subcutaneous injection of 90 mg/kg of xylenol orange (Sigma Chemical) 3 days prior to sacrifice. The mice were sacrificed 6 weeks post-fracture, and the right femora were harvested. The right femur was

dehydrated in graded concentrations of ethanol and embedded without decalcification in the modified methyl methacrylate (MMA) using our previously established protocol [20]. Briefly, the femur was dehydrated in 70%, 85%, 90%, and 100% graded ethanol and then submerged in xylene for three times. Thereafter, the femur was submerged in MMA-I (60% methlyl methacrylate, 35% butyl methacrylate, 3.8% methyl benzoate, and 1.2% polyethylene glycol), MMA-II (0.4 g of benzoyl peroxide added per 100 ml of MMA-I) and MMA-III (0.8 g of benzoyl peroxide added per 100 ml of MMA-I) in turn. Finally, the femur was solidified in the MMA-III with the addition of the accelerator *N*,*N*-dimthyl-*p*-toluidine. Sagittal sections for calluses were obtained from the right femur at a thickness of 15 μm using a Leica SM2500E microtome (Leica Microsystems, Germany). The mineral apposition rate (MAR), was calculated using professional image analysis software (Image J, NIH, USA) under fluorescence microscope (Leica image analysis system, Q500MC) [21].

Mechanical testing

The mechanical properties of the femora were examined at 4 and 6 weeks post-fracture using a three-point bending test. Before mechanical testing, the femur was taken out of the freezer and thawed overnight at the air-conditioned room temperature of 22°C. A material test machine (H25KS; Hounsfield Test Equipment, UK) with a 50 N load cell was used to test the femur to failure. The femora were positioned horizontally with the anterior surface upwards, centered on the supports with 10-mm distance. Load was constantly applied at the fracture site with a displacement rate of 5 mm/min that was directed vertically to mid-shaft with anterior surface upward. After failure, the load versus displacement curves were recorded. The ultimate load (UL) stiffness and the energy-to-failure values were calculated using built-in software (QMAT Professional; Tinius Olsen, Horsham, PA, USA) [22]. Contralateral intact femora harvested from both groups were evaluated by the same protocol [22]. The relative UL, stiffness, and energy-to-failure values of the callus were normalized to those of the intact femur.

Quantitative real-time PCR

Callus samples were isolated from the fracture sites 3 mm above and 3 mm below the fracture line. The samples were frozen in liquid nitrogen, pulverized using a Mikro-Dismembrator (Sartorius Stedim Biotech, Aubagne Cedex, France), and total RNA was isolated using the RNeasy® Mini Kit (QIAGEN, Dusseldorf, Germany). The concentration of total RNA was determined using a spectrophotometer. cDNA was synthesized from 0.5 μg of total RNA using a commercial first-strand cDNA synthesis kit (QIAGEN). Reverse transcription PCR was performed using primers specific for amplification of murine Col1a1, Col2a1, collagen type X (ColX), OC, and TRAP (see Table 1 for specific primer sequences). Col1a1 is the major bone matrix protein, Col2a1 is maximally expressed during chondrocyte proliferation, ColX peaks during terminal differentiation of chondrocytes, OC is expressed in fully matured osteoblasts and TRAP is expressed by osteoclasts during the resorptive process. Real-time PCR reactions were performed using SYBR Green in a 7900HT Fast Real-Time PCR System (Applied Biosystems, Foster City, CA, USA). The β-actin was selected as internal control and all gene expression levels were normalized to their baseline levels before fracture.

Analysis of bone formation and resorption markers

Sera were assayed for circulating levels of procollagen type I N-terminal propeptide (PINP), which is a bone formation marker, and C-terminal telopeptide of type I collagen (CTX), which is a bone resorption marker, by ELISA (IDS, Boldon, UK) following our previous established protocol [23]. Briefly, 50 μl of serum was added to a polyclonal rabbit anti-P1NP or anti-CTX-coated plate in duplicate and incubated with 50 μl of biotin-labeled P1NP or CTX for 1 h. Then, 150 μl of avidin-linked horseradish peroxidase was added to each well and incubated for 30 min. Finally, 150 μl of tetramethylbenzidine substrate was added for color development, which was measured using a microplate reader within 30 min of adding the stop solution. Standard curves were generated using serial

Table 1 Oligonucleotide primer sequences for real-time PCR analysis of gene expression

Target gene	Forward primer	Reverse primer
β-actin	5′-AGATGTGGATCAGCAAGCAG-3′	5′-GCGCAAGTTAGGTTTTGTCA-3′
Col1a1	5′-ACGTCCTGGTGAAGTTGGTC-3′	5′-CAGGGAAGCCTCTTTCTCCT-3′
Col2a1	5′-ACTGGTAAGTGGGGCAAGAC-3′	5′-CCACACCAAATTCCTGTTCA-3′
ColX	5′-ACCCCAAGGACCTAAAGGAA-3′	5′-CCCCAGGATACCCTGTTTTT-3′
Osteocalcin	5′-GCAGGAGGGCAATAAGGT-3′	5′-CGTAGATGCGTTTGTAGGC-3′
TRAP	5′-CAGCCCAAAATGCCTCGA-3′	5′-GCTTTTTGAGCCAGGACAGC-3′

dilutions of the P1NP or CTX calibration standards supplied in the ELISA kit [24], and the values were normalized to the baselines before fracture.

Statistical analysis

Data were expressed as the means ± SE, and were analyzed by two-way ANOVA with a least significant difference (LSD) post hoc test. All statistical analyses were performed using SPSS software, version 16.0 (SPSS, Chicago, IL). *P* values less than 0.05 were considered significant.

Results

Radiographic analysis

Radiopaque external callus around the fracture site was observed 1 week post-fracture in both groups. The space of the callus gaps decreased gradually with the fracture healing process at the weekly follow-up. As shown in the serial radiographs (Fig. 1c), the KO groups showed larger callus size and better callus structure than WT groups. Quantitative analysis showed that callus area increased from week 1 and reached the peak on week 2. After this point, the callus area decreased until week 6. Significantly higher callus area of KO than that of WT was shown on week 2, 3 and 4. After that, the difference was not significant (Fig. 1b).

Micro-CT angiography

The 3D angiograms generated from micro-CT analyses of fracture calluses generally demonstrated that there were more vessels and better structures in the KO mice than in the WT mice (Fig. 2a). Significantly larger vessel volumes and vessel volume fractions, along with a trend toward increased average vessel diameter (P=0.073), were detected in the fracture calluses of KO mice when compared with WT mice 1 week after surgery. Two weeks after fracture, the vessel volume, vessel diameter, and vessel volume fraction were all significantly higher in the KO mice than in the WT mice (Fig. 2b).

Micro-CT analysis of callus

At different time points, the reconstructed mineralized calluses showed different morphological characteristics between groups in the 3D micro-CT images (Fig. 3). At 1 week post-fracture, no significant mineralized callus appeared in either group. The quantitative measurements of TV and BV_l showed higher values in the KO group, although the differences were not statistically significant (Table 2). At 2 weeks post-fracture, remarkable callus formation was observed in both groups while the KO group showed larger callus sizes with smaller callus gaps at the fracture site (Fig. 3). Quantitatively, TV, BV_t, BV_l, BV_l/TV and BMC were significantly larger in the KO group than in the WT group at this time point (Table 2). At 4 weeks post-fracture, the callus gaps were bridged by mineralized callus in the KO group, compared with the active bone formation in the WT group (Fig. 3). The KO group presented higher BV_l, BV_l/TV, and BMC than the WT group (Table 2). At 6 weeks post-fracture, both groups entered the remodeling phase. The KO group demonstrated more smooth cortical surfaces compared with the WT group (Fig. 3). Quantitatively, KO group still had larger BV_l, BV_l/TV, and BMC than the WT group, but the difference became insignificant.

Histological and dynamic histomorphometric analysis

At 1 week post-fracture, there was a predominance of soft tissue reaction composed of a mixture of hematoma and granulation tissues in both the WT and the KO groups (Fig. 4a). At week 2, the callus appeared to bridge the fracture gap, and cartilaginous tissue filled the fracture site in both groups. The TCA, CCA, and cartilaginous callus fraction were all significantly higher in the KO mice compared with the WT mice, as evidenced by quantitative analysis in Safranin O-stained slices. At week 4, the cartilaginous callus became mineralized and lamellar bone was formed in both groups. The TCA and CCA were still significantly higher in the KO mice compared to the WT mice, but the difference in the cartilaginous callus fraction became insignificant (Fig. 4b). At week 6, the callus was remodeled and the size was decreased. There was no significant morphological difference between two groups, but dynamic bone histomorphometric analysis showed a higher MAR in the KO mice compared with the WT mice (Fig. 5a and b).

Mechanical testing of the callus

The results of the biomechanical analysis of the callus at 4 and 6 weeks after fracture were shown in Fig. 5 c–e. At 4 weeks post-surgery, the relative UL, stiffness, and energy-to-failure values of the callus from the KO mice were significantly higher than that in the WT mice. At 6 weeks post-surgery, there were no significant differences in mechanical properties found between the KO group and the WT group, including relative UL, stiffness, and energy to failure (Fig. 5 c–e).

Quantitative real-time PCR analysis of gene expression during fracture healing

In WT and KO mice, the mRNA expression levels of Col1a1, Col X, and TRAP steadily increased from week 1,

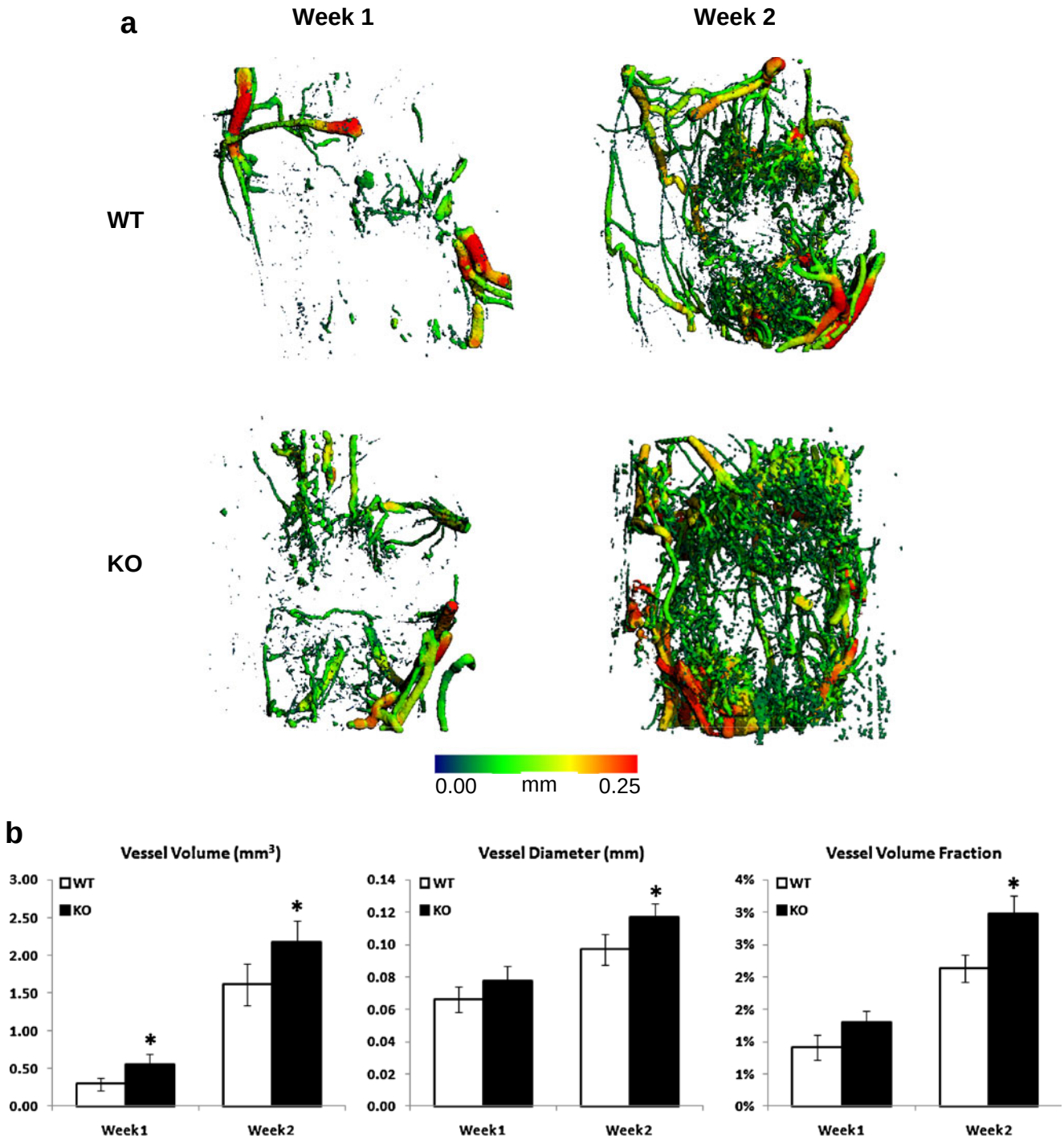

Fig. 2 Analysis of the vessel volume, vessel diameter and vessel volume fraction in fracture sites. **a** Representative 3D angiographs comparing the vessel-like structures in the fracture sites at week 1 and week 2 post-fracture between WT and KO mice, respectively. The *color* indicates the thickness (mm) of the vessel-like structures. **b** Quantification of the vessel volume, vessel diameter, and vessel volume fraction of callus at weeks 1 and 2. $N=4$ for each group, $^{*}P<0.05$ for comparison between WT and KO group at same time point by a two-way ANOVA with a LSD post hoc test

peaked at week 4, and then decreased from week 4 to week 6. The OC expression level increased from week 1, reached a plateau from week 2 to week 4, and finally decreased at week 6. Col1a1, Col X and OC mRNA expression levels were significantly higher in the KO mice than in the WT mice at weeks 2 and 4, but TRAP mRNA expression level was only significantly higher in the KO mice at week 4. The mRNA expression pattern of Col 2a1 followed the

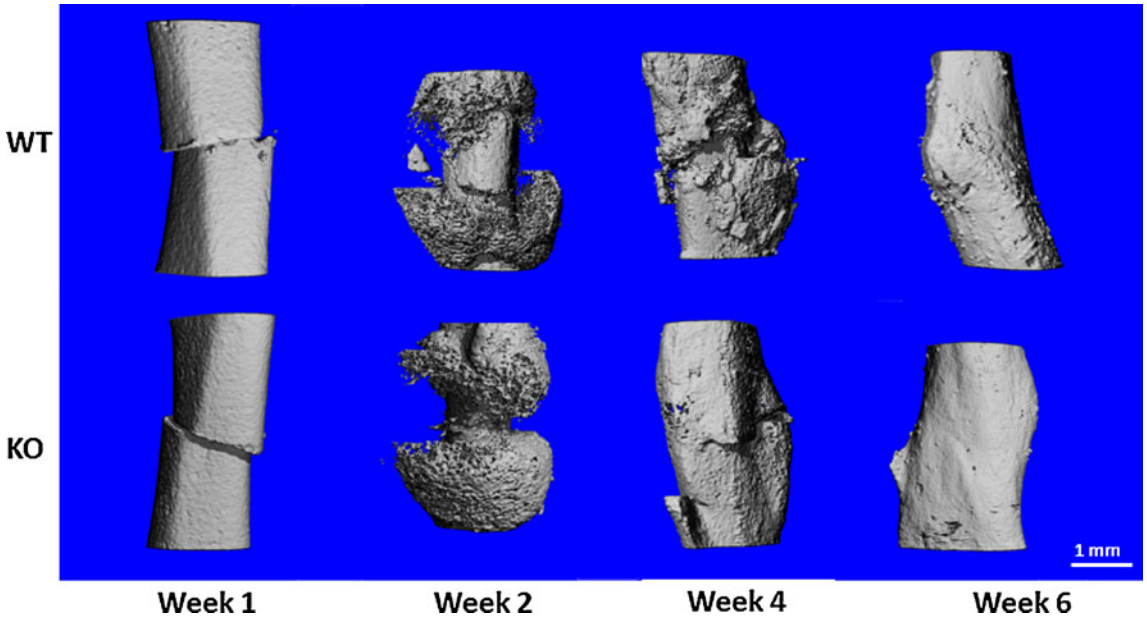

Fig. 3 Micro-CT analysis of fracture healing. Representative 3D images generated from micro-CT analysis of callus healing in WT and KO mice after fracture

same trend as the other genes except that it peaked at week 2, and the KO mice also showed significantly higher expression levels of Col2a1 than in the WT at weeks 2 and 4. At weeks 1 and 2, VEGF mRNA expression levels were significantly higher in the KO mice compared with the WT mice, but at weeks 4 and 6, VEGF mRNA expression levels in both groups were decreased and the difference became not significant (Fig. 6a)

Analysis of bone formation and resorption markers during bone healing

Circulating P1NP levels steadily increased from week 1, peaked at week 4, and then decreased from week 4 to week 6 in both groups. At weeks 2 and 4, circulating P1NP levels in the KO mice were significantly higher than in the WT mice. The circulating CTX levels in the both groups steadily increased from week 1 to week 4 and decreased thereafter. The levels of CTX were also significantly higher in the KO mice than in the WT mice at weeks 2 and 4 (Fig. 6b).

Discussion

In this study, we compared for the first time the differences in temporal and spatial changes of femoral open fracture healing between ERbeta KO mice and WT mice. It was demonstrated that fracture healing was enhanced in angiogenesis, osteogenesis, and mechanical

Table 2 Micro-CT analysis of fracture callus at varies time point

Parameter	WT	KO	WT	KO	WT	KO	WT	KO
TV (mm3)	7.64±0.21	8.20±0.68	21.18±7.77	30.43±7.11 *	18.75±5.11	20.40±3.43	16.66±3.18	15.24±1.69
BV_t (mm3)	4.61±0.19	4.99±0.69	11.01±4.04	15.41±3.18 *	8.65±1.31	9.70±1.63	6.50±0.93	7.06±1.17
BV_h (mm3)	2.84±0.18	2.87±0.45	3.95±0.45	4.29±0.48	4.21±0.40	3.95±0.54	3.28±0.54	3.75±0.57
BV_l (mm^3)	1.78±0.15	2.12±0.21	7.06±3.63	11.12±3.07 *	4.44±0.94	5.97±1.19 *	3.22±0.70	3.31±0.76
BV_t/TV (%)	60.40±3.02	60.9425±6.83	52.16±1.72	51.28±9.05	48.23±9.73	48.15±8.16	40.21±8.40	46.62±7.59
BV_h/TV (%)	37.11±2.56	35.13±5.54	20.57±6.22	14.74±6.63	23.81±5.84	19.83±4.07	20.7±6.42	24.97±5.13
BV_l/TV (%)	23.29±0.96	25.81±2.06	31.59±5.63	36.57±7.56 *	24.42±3.34	29.31±3.96 *	19.51±2.83	21.65±3.68
BMC (mg HA)	3.82±0.16	3.97±0.61	6.23±1.72	8.62±1.26*	5.23±0.72	6.62±0.91*	3.68±0.63	4.37±0.87

TV Total tissue volume, BV_t Total bone volume, BV_h volume of high-density bone, BV_l volume of low-density bone, *BMC* bone mineral content
*$P<0.05$ compared to WT group; two-way ANOVA with LSD post hoc test. Mean±SD ($N=8$)

properties. It indicated ERbeta play an important role in fracture healing.

Angiogenesis

Angiogenesis is an essential stage of bone healing; previous studies demonstrated that angiogenic factors, such as VEGF, were required for bone formation during bone healing [25]. Micro-CT based angiography demonstrated that there were more vessels with better structures in the KO mice than in the WT mice at both weeks 1 and 2. This result was also supported by significantly higher VEGF mRNA expression levels at weeks 1 and 2. Taken together, our data indicated that angiogenesis was enhanced during fracture healing in the KO mice when compared with the WT mice. This result implied that ERbeta inhibited angiogenesis during fracture healing. These results were consistent with a previous research on breast cancer that demonstrated a repressive effect of ERbeta in VEGF mRNA expression [14]. One recent study demonstrated that ERbeta could inhibit hypoxia-inducible factor-1 (HIF-1) activity and further downregulate VEGF expression. It was correlated with ERbeta's ability to degrade aryl hydrocarbon receptor nuclear translocator (ARNT) via ubiquitylation processes [26]. This finding might explain the inhibitory effect of ERbeta in angiogenesis found in the present study.

Fracture healing

Serial radiography, micro-CT reconstruction, and histological examination consistently demonstrated a larger callus size in KO mice than in the WT mice. Quantitative micro-CT and histology showed that low-density bone or cartilaginous area was also higher in the KO mice than in the WT mice, suggesting that endochondral ossification was enhanced during fracture healing in ERbeta KO bones. Dynamic bone histomorphometry also showed faster new bone formation supported by a higher MARs in the KO mice. The observed increase in Col1a1, Col2a1, Col X, and OC mRNA expression and in bone formation biomarker P1NP expression in the KO mice when compared with the WT mice suggested that the activation of osteoprogenitor cells was enhanced in the KO mice. These changes likely contributed to the enhanced bone formation in the ERbeta KO mice during fracture healing.

During the late phase of bone healing, the callus in the fracture site was fully remodeled into a cortical-like structure in both groups, as evidenced by both micro-CT data and histological examination. These results indicated that the remodeling capability from woven bone to lamellar bone was not affected in the ERbeta KO mice. In the present study, the use of relative bone resorption levels to the baseline was aimed to reflect local bone resorption during bone healing after diminishing the systemic factors. It is known that bone resorption is coupled with bone formation in normal bone physiology. In the present study, bone formation level from the local callus was higher in the KO mice than the WT mice at weeks 2 and 4. Therefore, the local expression levels of bone resorption marker CTX were also higher in the KO mice at week 2 and week 4. Additionally, the levels of TRAP mRNA from the local callus tissue were also consistently significantly higher in the KO mice at week 4. In terms of mechanical properties, the KO mice had faster restoration capability than the WT mice at week 4, as evidenced by a higher percent recovery with respect to the UL,stiffness and the energy-to-failure in KO mice when compared with WT mice.

Most of the parameters showed significant differences between groups at week 4 that were, however, no more detectable at week 6. From histology and micro-CT analysis, we found that the callus was entering remodeling phase at week 4, and both the structure and the mechanical properties almost restored close to intact bone at week 6. Given time extension, it is not surprising that fracture in both groups would heal and show no difference after entering into remodeling phase, such as week 6 in the present study. This result was also consistent with previously reported mouse fracture healing studies that demonstrated no difference in the later healing time point. [18, 27, 28]

ER beta and endochondral ossification

Fracture repair is a specialized postnatal repair process that recapitulates aspects of embryological skeletal development. Endochondral ossification is a very important process in both longitudinal bone growth and bone healing. A previous transgenic mouse study showed that KO of ERbeta in female mice induced an increase in longitudinal bone growth compared with the WT mice [11, 12, 29]; female ERalpha KO mice that still expressed ERbeta had shorter bones than female ERalpha and ERbeta double KO mice (DERKO) [9, 12]. Moreover, ERbeta has a demonstrated capacity for mediating growth plate fusion in female mice [9]. All previous studies confirm that ERbeta can inhibit endochondral ossification in bone development. In the current study, we also demonstrated that knock of ERbeta induces Col X expression, a specific marker for chondrocyte hypertrophy and VEGF, a marker for angiogenesis. These data indicate KO ERbeta accelerate bone fracture healing by stimulating chondrocyte terminal differentiation and the endochondral ossification.

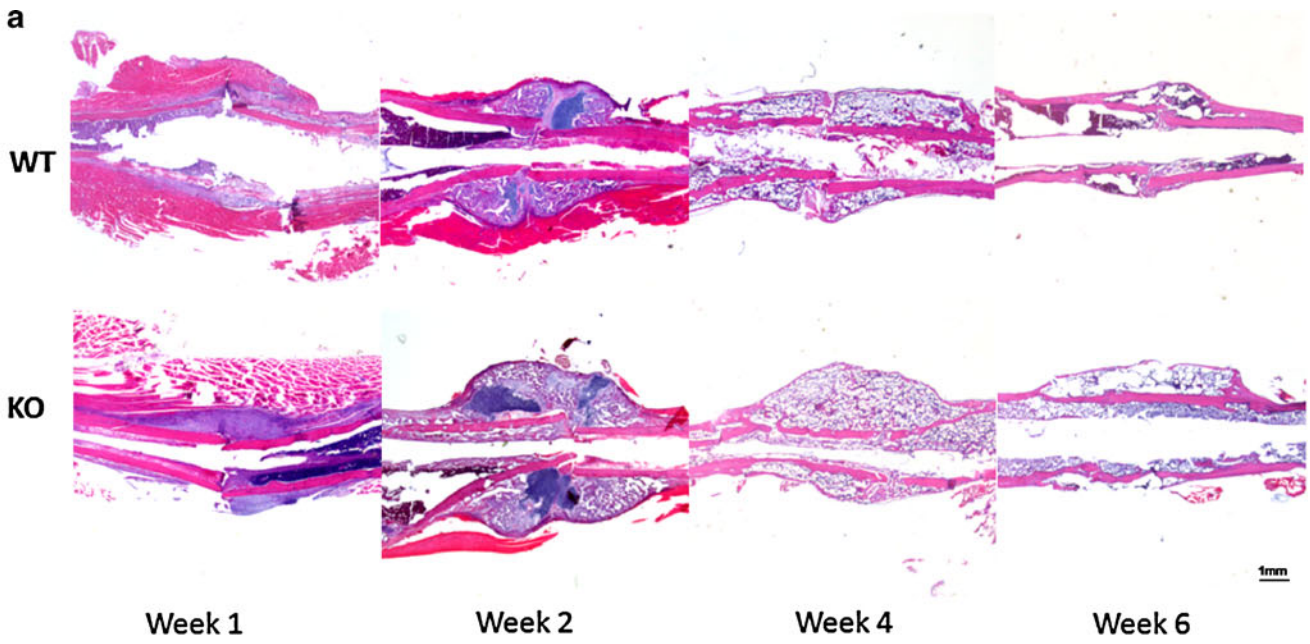
a
WT
KO
1mm
Week 1
Week 2
Week 4
Week 6

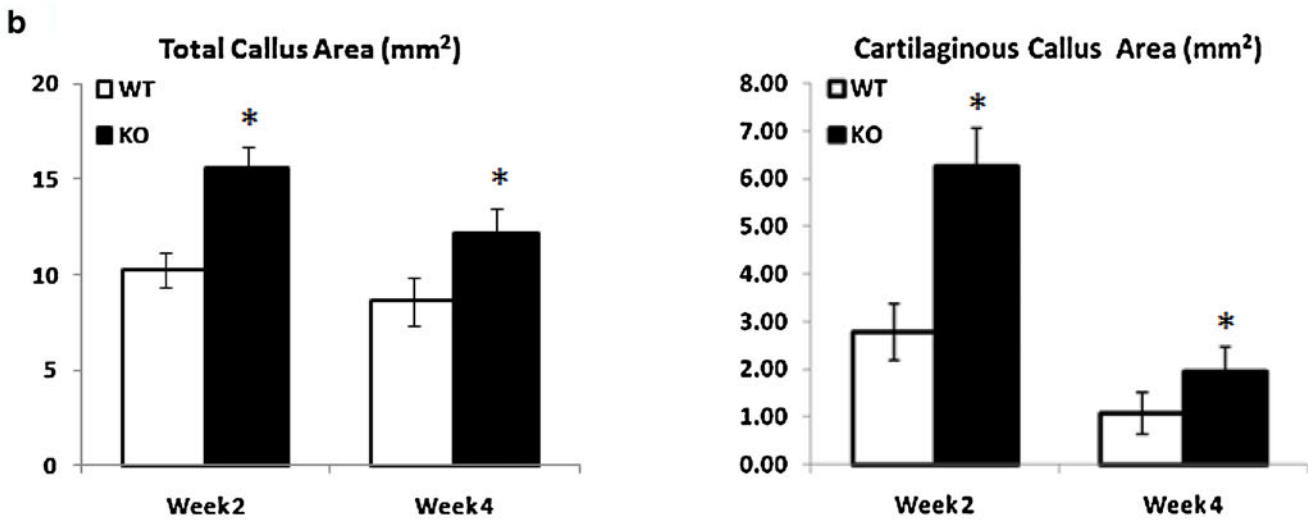
b
Total Callus Area (mm²)
WT
KO
20
15
10
5
0
*
*
Week2
Week4
Cartilaginous Callus Area (mm²)
8.00
7.00
6.00
5.00
4.00
3.00
2.00
1.00
0.00
*
*
Week2
Week4

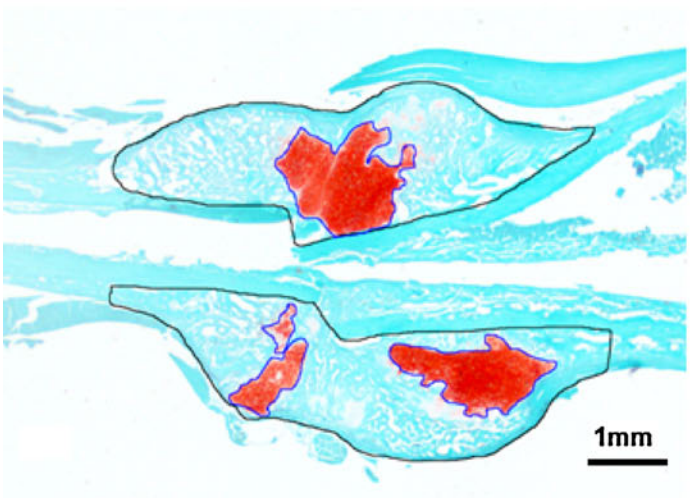
1mm

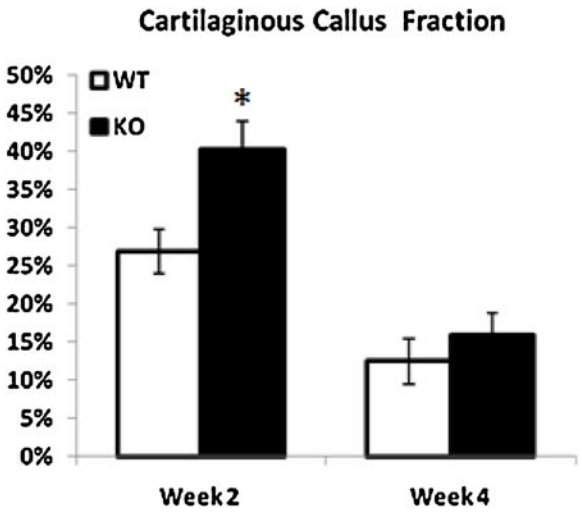
Cartilaginous Callus Fraction
WT
KO
50%
45%
40%
35%
30%
25%
20%
15%
10%
5%
0%
*
Week2
Week4

Fig. 4 Histological analysis of the progression of fracture healing in WT and KO mice with representative photomicrographs of callus sections. **a** Callus sections stained with H&E for general observation of fracture calluses at various healing time points (10× magnification). **b** Callus sections stained with Safranin O: *black line* indicated the TCA and *blue line* indicated CCA.TCA, CCA, and cartilaginous callus fraction were quantified in both the WT and KO groups at weeks 2 and 4. The images were acquired at 10× magnification. $N=8$ for each group, $^*P<0.05$ for comparison between WT and KO group at same time point by a two-way ANOVA with a LSD post hoc test

ER beta in aged fracture

Delayed or impaired bone regeneration in the elderly is common [30]. Our unpublished clinical biopsy data showed that the ERbeta mRNA expression levels in the callus of elderly were much higher than in corresponding young people. The dysregulated ERbeta expression should be considered when impaired fracture healing is observed in aged population. In the present study, we demonstrated that a KO of ERbeta could enhance the fracture healing in the normal bone. Therefore, we further hypothesize that the inhibition of ERbeta could promote aged fracture healing. Currently, we are using both genetic and pharmacological approach to block ERbeta, and we are evaluating the effects on fracture healing in an aged mouse model. If the hypothesis could be supported, the inhibition of ERbeta can be considered another therapeutic strategy for aged fracture healing.

Conclusions

In this study, we elucidated for the first time the role of ERbeta in female femoral open fracture healing. We

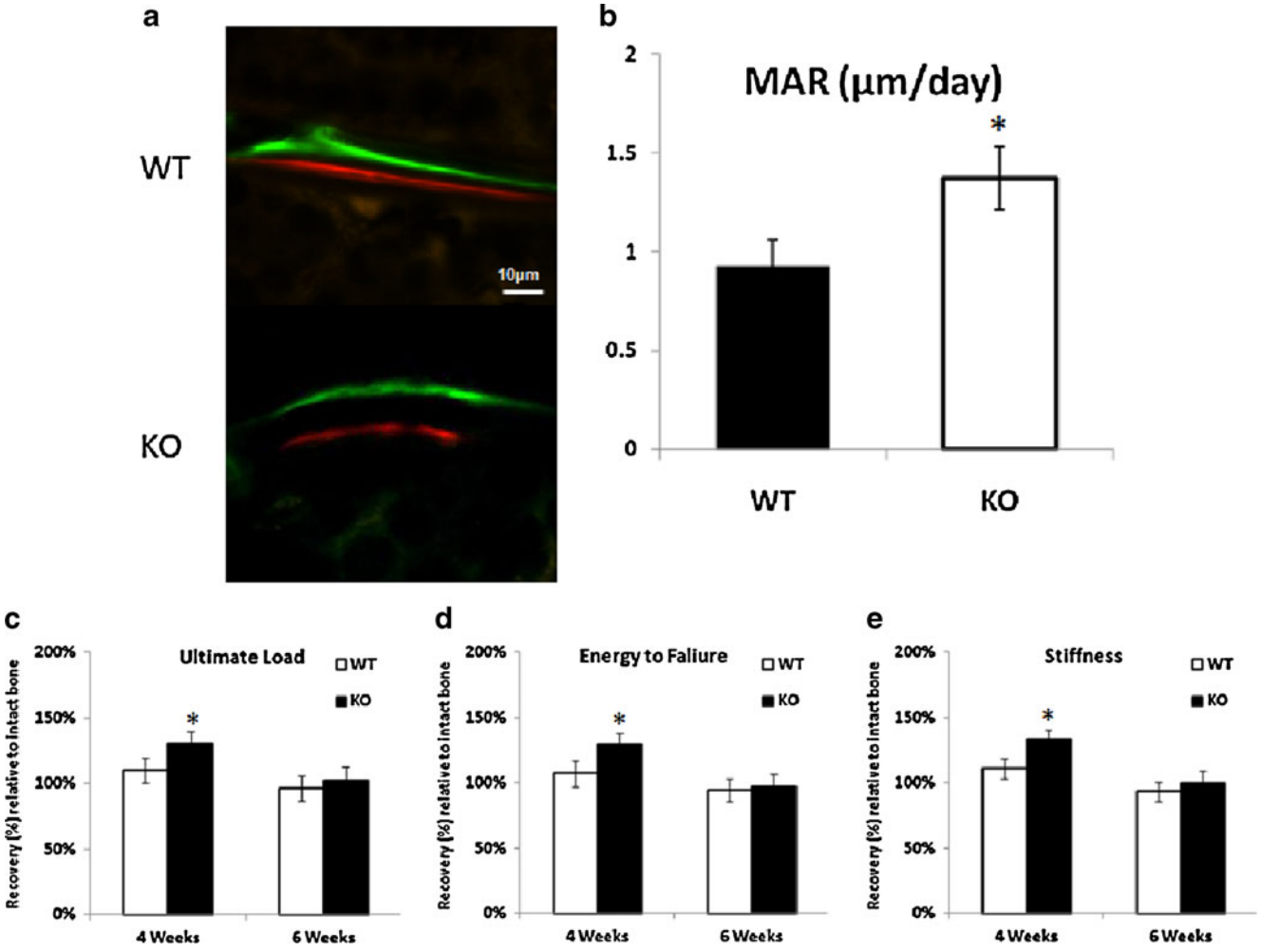

Fig. 5 Dynamic histomorphometric analysis and mechanical testing results. **a** Double-labeled fluorescence dye at the fracture site 6 weeks post-surgery. **b** Quantification of MAR in both WT and KO groups, at 6 weeks post-surgery. **c–e** Data reflect the average load, stiffness, and energy-to-failure values of the callus relative to the contralateral intact femur at weeks 4 and 6. $N=4$ for dynamic histomorphometric analysis and $N=8$ for mechanical testing, $^*P<0.05$ for comparison between WT and KO group at same time point by a two-way ANOVA with a LSD post hoc test

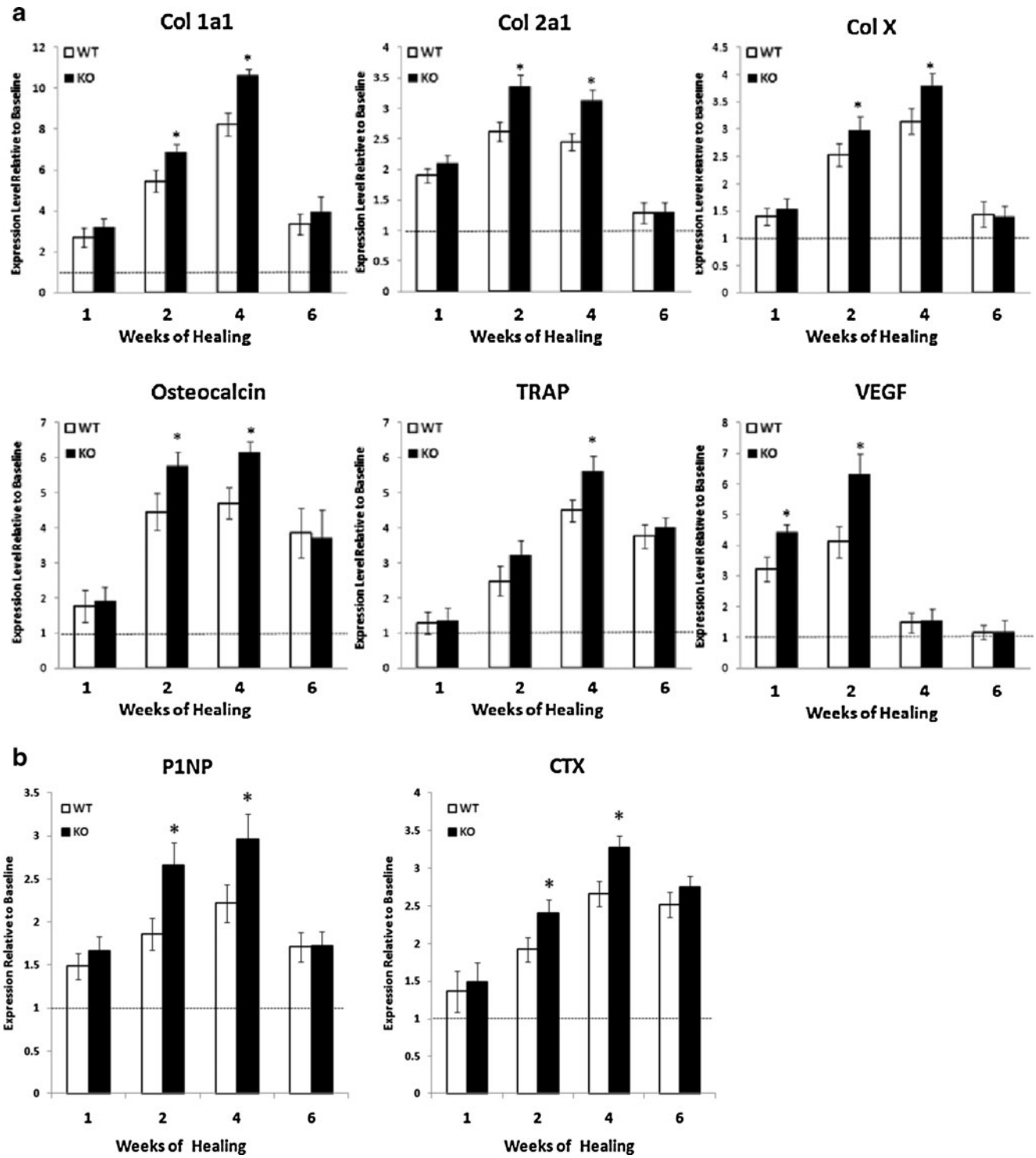

Fig. 6 Temporal analysis of callus gene expression and serum biochemical markers. **a** Temporal changes in Col1a1, Col2a1, Col X, OC, TRAP, VEGF mRNA expression in callus samples following fracture surgery determined by quantitative RT-PCR analysis with expression levels normalized to that of β-actin. **b** Concentrations of serum bone formation marker P1NP and serum bone resorption marker CTX determined by ELISA. $N=4$ for mRNA expression and $N=8$ for serum biochemical markers, $^{*}P<0.05$ for comparison between WT and KO group at same time point by a two-way ANOVA with a LSD post hoc test

demonstrated that fracture healing was enhanced in the early stage of neovascularization and middle stage of endochondral ossification but not by the end of healing. Our findings might suggest that blockade of ERbeta could be a potential therapeutic strategy for fracture healing.

Acknowledgments This study was supported by AO Research Grant (S-08-74Z) and CUHK Direct Grant (2008.1.063). We also thank Mr. Wang Yu-Gang for his support in animal care.

Conflicts of interest None.

References

1. Ferguson C, Alpern E, Miclau T, Helms JA (1999) Does adult fracture repair recapitulate embryonic skeletal formation? Mech Dev 87:57–66
2. Einhorn TA (1998) The cell and molecular biology of fracture healing. Clin Orthop Relat Res S7–S21
3. Gerstenfeld LC, Cho TJ, Kon T, Aizawa T, Tsay A, Fitch J, Barnes GL, Graves DT, Einhorn TA (2003) Impaired fracture healing in the absence of TNF-alpha signaling: the role of TNF-alpha in endochondral cartilage resorption. J Bone Miner Res 18:1584–1592
4. Einhorn TA (2005) The science of fracture healing. J Orthop Trauma 19:S4–S6
5. Turner RT, Riggs BL, Spelsberg TC (1994) Skeletal effects of estrogen. Endocr Rev 15:275–300
6. Beil FT, Barvencik F, Gebauer M, Seitz S, Rueger JM, Ignatius A, Pogoda P, Schinke T, Amling M (2010) Effects of estrogen on fracture healing in mice. J Trauma 69:1259–1265
7. Kuiper GG, Enmark E, Pelto-Huikko M, Nilsson S, Gustafsson JA (1996) Cloning of a novel receptor expressed in rat prostate and ovary. Proc Natl Acad Sci USA 93:5925–5930
8. Green S, Walter P, Greene G, Krust A, Goffin C, Jensen E, Scrace G, Waterfield M, Chambon P (1986) Cloning of the human oestrogen receptor cDNA. J Steroid Biochem 24:77–83
9. Chagin AS, Lindberg MK, Andersson N, Moverare S, Gustafsson JA, Savendahl L, Ohlsson C (2004) Estrogen receptor-beta inhibits skeletal growth and has the capacity to mediate growth plate fusion in female mice. J Bone Miner Res 19:72–77
10. Ke HZ (2005) In vivo characterization of skeletal phenotype of genetically modified mice. J Bone Miner Metab 23(Suppl):84–89
11. Ke HZ, Brown TA, Qi H, Crawford DT, Simmons HA, Petersen DN, Allen MR, McNeish JD, Thompson DD (2002) The role of estrogen receptor-beta, in the early age-related bone gain and later age-related bone loss in female mice. J Musculoskelet Neuronal Interact 2:479–488
12. Lindberg MK, Alatalo SL, Halleen JM, Mohan S, Gustafsson JA, Ohlsson C (2001) Estrogen receptor specificity in the regulation of the skeleton in female mice. J Endocrinol 171:229–236
13. Windahl SH, Vidal O, Andersson G, Gustafsson JA, Ohlsson C (1999) Increased cortical bone mineral content but unchanged trabecular bone mineral density in female ERbeta(−/−) mice. J Clin Invest 104:895–901
14. Hartman J, Lindberg K, Morani A, Inzunza J, Strom A, Gustafsson JA (2006) Estrogen receptor beta inhibits angiogenesis and growth of T47D breast cancer xenografts. Cancer Res 66:11207–11213
15. Doyon AR, Ferries IK, Li J (2010) Glucocorticoid attenuates the anabolic effects of parathyroid hormone on fracture repair. Calcif Tissue Int 87:68–76
16. He YX, Zhang G, Pan XH, Liu Z, Zheng LZ, Chan CW, Lee KM, Cao YP, Li G, Wei L, Hung LK, Leung KS, Qin L (2011) Impaired bone healing pattern in mice with ovariectomy-induced osteoporosis: a drill-hole defect model. Bone 48:1388–1400
17. Zhang G, Sheng H, He YX, Xie XH, Wang YX, Lee KM, Yeung KW, Li ZR, He W, Griffith JF, Leung KS, Qin L (2009) Continuous occurrence of both insufficient neovascularization and elevated vascular permeability in rabbit proximal femur during inadequate repair of steroid-associated osteonecrotic lesions. Arthritis Rheum 60:2966–2977
18. Duvall CL, Taylor WR, Weiss D, Wojtowicz AM, Guldberg RE (2007) Impaired angiogenesis, early callus formation, and late stage remodeling in fracture healing of osteopontin-deficient mice. J Bone Miner Res 22:286–297
19. Hao YJ, Zhang G, Wang YS, Qin L, Hung WY, Leung K, Pei FX (2007) Changes of microstructure and mineralized tissue in the middle and late phase of osteoporotic fracture healing in rats. Bone 41:631–638
20. Qin L, Hung L, Leung K, Guo X, Bumrerraj S, Katz L (2001) Staining intensity of individual osteons correlated with elastic properties and degrees of mineralization. J Bone Miner Metab 19:359–364
21. Songlin P, Ge Z, Yixin H, Xinluan W, Pingchung L, Kwoksui L, Ling Q (2009) Epimedium-derived flavonoids promote osteoblastogenesis and suppress adipogenesis in bone marrow stromal cells while exerting an anabolic effect on osteoporotic bone. Bone 45:534–544
22. Zhang G, Qin L, Hung WY, Shi YY, Leung PC, Yeung HY, Leung KS (2006) Flavonoids derived from herbal *Epimedium brevicornum* Maxim prevent OVX-induced osteoporosis in rats independent of its enhancement in intestinal calcium absorption. Bone 38:818–825
23. He YX, Zhang G, Pan XH, Liu Z, Zheng LZ, Chan CW, Lee KM, Cao YP, Li G, Wei L, Hung LK, Leung KS, Qin L (2011) Impaired bone healing pattern in mice with ovariectomy-induced osteoporosis: A drill-hole defect model. Bone 48:1388–1400
24. Rauner M, Stupphann D, Haas M, Fert I, Glatigny S, Sipos W, Breban M, Pietschmann P (2009) The HLA-B27 transgenic rat, a model of spondyloarthritis, has decreased bone mineral density and increased RANKL to osteoprotegerin mRNA ratio. J Rheumatol 36:120–126
25. Jacobsen KA, Al-Aql ZS, Wan C, Fitch JL, Stapleton SN, Mason ZD, Cole RM, Gilbert SR, Clemens TL, Morgan EF, Einhorn TA, Gerstenfeld LC (2008) Bone formation during distraction osteogenesis is dependent on both VEGFR1 and VEGFR2 signaling. J Bone Miner Res 23:596–609
26. Lim W, Park Y, Cho J, Park C, Park J, Park YK, Park H, Lee Y (2011) Estrogen receptor beta inhibits transcriptional activity of hypoxia inducible factor-1 through the downregulation of arylhydrocarbon receptor nuclear translocator. Breast Cancer Res 13: R32
27. Holstein JH, Menger MD, Scheuer C, Meier C, Culemann U, Wirbel RJ, Garcia P, Pohlemann T (2007) Erythropoietin (EPO): EPO-receptor signaling improves early endochondral ossification and mechanical strength in fracture healing. Life Sci 80:893–900
28. Colburn NT, Zaal KJ, Wang F, Tuan RS (2009) A role for gamma/delta T cells in a mouse model of fracture healing. Arthritis Rheum 60:1694–1703
29. Windahl SH, Hollberg K, Vidal O, Gustafsson JA, Ohlsson C, Andersson G (2001) Female estrogen receptor beta−/− mice are partially protected against age-related trabecular bone loss. J Bone Miner Res 16:1388–1398
30. Gruber R, Koch H, Doll BA, Tegtmeier F, Einhorn TA, Hollinger JO (2006) Fracture healing in the elderly patient. Exp Gerontol 41:1080–1093